



### **Science Arts & Métiers (SAM)**

is an open access repository that collects the work of Arts et Métiers Institute of Technology researchers and makes it freely available over the web where possible.

This is an author-deposited version published in: <https://sam.ensam.eu>  
Handle ID: <http://hdl.handle.net/10985/6797>

#### **To cite this version :**

Camille ROBERT, Arnaud DELAMEZIERE, Philippe DAL SANTO, Jean-Louis BATOZ -  
Comparison between incremental deformation theory and flow rule to simulate sheet-metal  
forming processes - Journal of Materials Processing Technology p.p. 1123–1131 - 2012

Any correspondence concerning this service should be sent to the repository

Administrator : [scienceouverte@ensam.eu](mailto:scienceouverte@ensam.eu)



# Comparison between incremental deformation theory and flow rule to simulate sheet metal forming processes

C. Robert<sup>a,b,\*</sup>, A. Delamézière<sup>b</sup>, P. Dal Santo<sup>a</sup>, J.L. Batoz<sup>c</sup>

<sup>a</sup>*Arts et Métiers ParisTech, LAMPA, 2 bd du Ronceray, 49035 Angers Cedex, France*

<sup>b</sup>*LEMTA, Nancy-Université, ERMeP, GIP-InSIC, 27 rue d'Heilleule, 88100 Saint-Dié-des-Vosges, France*

<sup>c</sup>*UTC, AVENUES-GSU, Centre Pierre Guillaumat 2, BP 60319, rue du Docteur Schweitzer, 60203 Compiègne Cedex, France*

---

## Abstract

Numerical simulation of the deep drawing process for the manufacture of aeronautical or automotive components should predict with good accuracy the behaviour during the forming operation, taking into account, the material and the process parameters. Existing simulation strategies give good results, however calculation time are long due to the high degree of non-linearities of these problems. The objective of this work is therefore to decrease the calculation time, resulting from the non-linear material behaviour. A new algorithm based on incremental deformation theory (related to Hencky Theory) is presented, in order to compute the plasticity rule in a finite element code (ABAQUS). This algorithm is used to simulate two sheet-metal forming processes: typical stretch forming operation and incremental single point sheet forming. For each case the new algorithm is compared with a classical flow rule plasticity law. In order to have a valid comparison in terms of CPU time, the two material behaviour laws have been implemented in ABAQUS EXPLICIT using the material user function (VUMAT). Good agreement in terms of the stress state and thickness distribution is obtained with the new approach. A significant decrease in CPU time is observed when the major source of non-linearity comes from the material behaviour.

**Keywords:** Sheet forming processes, plasticity, deformation theory, flow rule, stretch forming, incremental sheet forming

---

---

\*Corresponding author. Tel: +33 2 41 20 73 27; fax: +33 2 41 20 73 20  
Email address: [camille.robert@ensam.eu](mailto:camille.robert@ensam.eu) (C. Robert)

## General notations

$\{\}$  = vector

$\langle \rangle = \{\}^T$

$[]$  = matrix

$\Delta f$  = increment of  $f$

$\sigma_{eq}$  = equivalent stress

$\bar{\sigma}$  = yield stress

$\bar{\varepsilon}^{pl}$  = equivalent plastic strain

$\{\sigma_{11}, \sigma_{22}, \sigma_{12}\}$  = 2D stress component

$\{\varepsilon_{11}, \varepsilon_{22}, \gamma_{12}\}$  = 2D strain component

IDF : Incremental Deformation Formulation

FRF : Flow Rule Formulation

## 1. Introduction

Numerical simulations of industrial processes need to take into account non-linearities induced by the material behaviour, large displacements, large strains and contact phenomenon between the tools and the formed parts. These procedures are computationally intensive. One of the main objectives for designers and engineers faced with the simulation of industrial processes is the reduction of the CPU time in combination with an acceptable level of accuracy, in particular at the design stage.

This paper presents the implementation of a new algorithm to simulate elasto-plastic material behaviour with anisotropic plasticity criterion based on the incremental deformation theory in the ABAQUS commercial finite element code. The aim of the algorithm is to reduce the global CPU time for the numerical simulation of stretch forming and incremental sheet-metal forming processes. To determine the elasto-plastic state of the workpiece, two fundamental principles based on the theory of plasticity are used: (a) the theory of deformation and (b) the flow rule theory. The theory of deformation was initially developed by Hencky (1924). Alternatively, many authors, like Simo and Ortiz (1985), have presented algorithms which use the flow rule method to take into account the deformation path dependence. Lubarda (2000) showed that both theories are equivalent only under proportional loading. Today, the flow rule method is used in the majority of numerical simulations, leading to good agreement with experimental results.

The theory of deformation can be defined in terms of total deformation or incremental deformation. In the case of total deformation, the load grows proportionally to the time. Lemaitre and Chaboche (1988) proposed the following relationship:  $\sigma(M, t) = c(t) \cdot \sigma(M, t_f)$ . Where  $\sigma(M, t)$  is the stress tensor at material point  $M$  and at the time  $t$ ,  $t_f$  is the final time and  $c(t)$  is an increasing function of time. With this assumption, it is not possible to take into account unloading of the workpiece (i.e. springback cannot be predicted). Today, this theory is principally implemented in the Inverse Approach (for example by Guo et al. (2000) using DKT12 shell element or Na et al. (2011) using a membrane element model with bending modification based on element moment equilibrium). This approach is generally used for the optimisation of deep drawing processes, because the CPU time is less consuming than a dynamic explicit solver. The total deformation theory does not take into account the strain path because the state of stress is assumed to be proportional at all times during the simulation, and do not take into account the current yield surface normality.

In the incremental deformation theory, the loading is considered to be proportional only during one time increment. Chung and Richmond (1993) present this theory in which the total strain sub-increment is proportional to the fixed strain increment. An efficient algorithm, using this theory has been developed by Ramakrishnan et al. (1998) for isotropic material behaviour. Good results have been observed when compared to experimental results. The advantage of this theory, compared to the flow rule theory, is that it does not use an integration scheme, as discussed by Yang and Kim (1986).

This paper proposes an elasto-plastic algorithm with an anisotropic criterion and using the incremental deformation theory. The algorithm is tested for two sheet forming processes: stretch forming, and incremental sheet forming.

Stretch forming is a well established forming operation which is only really appropriate for large scale production due to the high tooling cost involved. However, the second process investigated, incremental single point sheet forming, is a relatively new process used to manufacture deep drawn components. The basic idea is to locally push the sheet with a hemispherical tool that follows a complex path. The advantage of this process is its great flexibility, because only one hemispheric tool is required in free bulging. It is also possible to use a die in order to increase the quality of the final geometry. The applied forces are not very high, so, the die can be manufactured with low cost materials. The major disadvantage of this process is that the forming time is very long. Therefore, incremental sheet forming is more appropriate for small scale production or for creating prototypes. These two sheet-metal forming processes were chosen due to their different loading conditions and

different material behaviour.

In terms of deep drawing, the Inverse Approach can quickly predict the thickness of the sheet at the end of the forming process, but the stress state is generally inaccurate. The results using dynamic explicit solvers are more accurate however the CPU time is very long. Therefore, the incremental deformation theory should reduce the CPU time, while maintaining good accuracy.

Considering the incremental sheet forming processes it is not possible to use a one step method due to the changes in the contact conditions between the tool and the sheet, during the simulation. In this case, the incremental deformation theory could also be used to reduce the CPU time.

In the following, a description of the classical plastic flow rule method and the new algorithm is given. The results of numerical simulation, using both plasticity theories are then presented for :

- a) the Nakazima test (stretch forming of an hemispherical cup), and
- b) The incremental forming of a cylindrical cup.

The results are subsequently discussed and some conclusions are presented.

## 2. The classical flow rule method

In this section, the numerical integration in relation with the flow rule method is presented. In this method, the yield surface normality rule is used to describe the evolution of strain during an increment of strain. Many authors have presented algorithms for this theory, including Crisfield (1991). The general constitutive equations defining the stress as a function of the elastic deformation are:

$$\{\sigma\} = [C^{el}] \{\varepsilon^{el}\} \quad (1)$$

where  $[C^{el}]$  is the elastic stiffness tensor. In the case of plane stress  $[C^{el}]$  reduces to:

$$[C^{el}] = \begin{pmatrix} \frac{E}{1-\nu^2} & \frac{\nu E}{1-\nu^2} & 0 \\ \frac{\nu E}{1-\nu^2} & \frac{E}{1-\nu^2} & 0 \\ 0 & 0 & \frac{E}{2(1+\nu)} \end{pmatrix} \quad (2)$$

The coefficients  $E$  and  $\nu$  are the Young modulus and the Poisson ratio respectively. The equivalent stress  $\sigma_{eq}$  is defined as:

$$\sigma_{eq} = (\langle \sigma \rangle [P] \{\sigma\})^{1/2} \quad (3)$$

where  $[P]$  takes into account the material anisotropy in the following form:

$$[P] = \begin{pmatrix} 1 & -\frac{r_0}{1+r_0} & 0 \\ -\frac{r_0}{1+r_0} & \frac{r_0(1+r_{90})}{r_{90}(1+r_0)} & 0 \\ 0 & 0 & 2r_{45}\frac{r_0+r_{90}}{r_{90}(1+r_0)} \end{pmatrix} \quad (4)$$

where  $r_0$ ,  $r_{45}$  and  $r_{90}$  are the Lankford coefficients.

The isotropic hardening law may be fitted by:

$$\bar{\sigma} = A + B \left( C + \bar{\varepsilon}^{pl} \right)^n \quad (5)$$

where the parameters  $A$ ,  $B$ ,  $C$  and  $n$  are determined experimentally by means of tensile tests.

The yield function  $f$ , according for the Hill 48 an isotropy criterion, is written as:

$$f = \sigma_{eq} - \bar{\sigma} \quad (6)$$

The generalised normal plastic flow rule gives the plastic strain increment in the form of:

$$\{\dot{\varepsilon}^{pl}\} = \frac{\dot{\varepsilon}^{pl}}{\bar{\varepsilon}^{pl}} \left\{ \frac{\partial f}{\partial \{\sigma\}} \right\} = \frac{\dot{\varepsilon}^{pl}}{\bar{\varepsilon}^{pl}} \frac{[P]\{\sigma\}}{\sigma_{eq}} \quad (7)$$

Using the consistency condition ( $df = 0$ ), the increment of the equivalent plastic strain rate  $\dot{\bar{\varepsilon}}^{pl}$  can be written as a function of the normal to the yield surface  $\left\{ \frac{\partial f}{\partial \{\sigma\}} \right\}$ , the hardening modulus  $\frac{\partial \bar{\sigma}}{\partial \bar{\varepsilon}^{pl}}$  and the strain rate  $\{\dot{\varepsilon}\}$ . This is lead to equation below:

$$\dot{\bar{\varepsilon}}^{pl} = \frac{\left\langle \frac{\partial f}{\partial \{\sigma\}} \right\rangle [C^{el}] \{\dot{\varepsilon}\}}{\left\langle \frac{\partial f}{\partial \{\sigma\}} \right\rangle [C^{el}] \left\{ \frac{\partial f}{\partial \{\sigma\}} \right\} + \frac{\partial \bar{\sigma}}{\partial \bar{\varepsilon}^{pl}}} \quad (8)$$

The first step in the classical algorithm is to make an elastic prediction, in wh ich the increment of deformation is considered to be purely elastic. If the yield function value is greater than zero, the radial return to the yield function is determined by iteration until convergence, that is, until the yield function value equal zero.

Figure 1 shows the evolution of the stress during these plastic iterations. The sub-script  $n$  represents the previous increment and  $n+1$  the end of the current increment. The superscript  $(i)$  represents the iteration  $i$ .

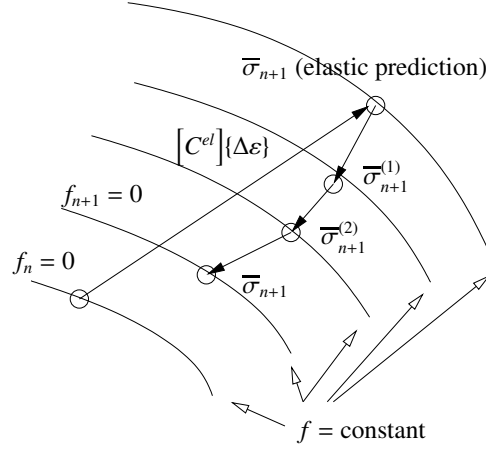


Figure 1: Flow rule theory, Simo and Ortiz (1985)

### 3. Incremental deformation theory – the new algorithm

In this section, the numerical integration of the incremental deformation theory is presented. In this study, the Hill48 criterion is used to describe the anisotropic behaviour of the sheet. This theory was initially proposed by Hencky (1924) based on the total deformation. In the present method, the load is proportionally increased during one increment of strain. In this case, it is possible to use equivalent variables (stress and strain) to describe the material behaviour because the increment of strain evolves according to a scalar function,  $\Delta\epsilon(t) = \alpha(t) \cdot \Delta\epsilon(t_0 + \Delta t)$  as discussed by Chung and Richmond (1993). Where  $\Delta\epsilon$  is the increment of the strain tensor,  $\Delta t$  is the time increment,  $t_0$  is the time at the beginning of the increment, and  $\alpha(t)$  is an increasing function of time. In this case, it is possible to take into account of the unloading.

Figure 2 shows the principle of the theory of the incremental deformation for a one-dimensional case.  $A$  is related to an initial state of stress and strain, and  $B$  is the state reached at the end of the increment.

The stress at state  $B$  is a function of the elastic strain at  $A$  ( $\epsilon_A^{el}$ ), the increment of deformation ( $\Delta\epsilon$ ) and of an elasto-plastic modulus  $E_{ep}$  which is a function of a plastic modulus  $E_p$  and Young modulus. For the uniaxial case  $\sigma_B$  is :

$$\sigma_B = E_{ep} (\epsilon_A^{el} + \Delta\epsilon) \quad (9)$$

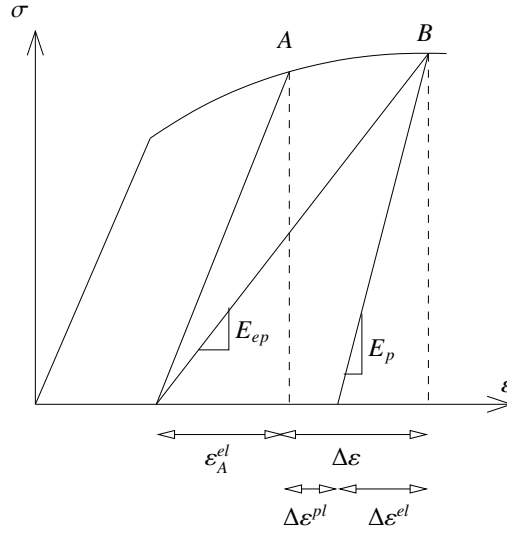


Figure 2: Principle of the incremental deformation theory, Ramakrishnan et al. (1998)

The strain tensor is computed using elastic and plastic parts:

$$\begin{cases} \{\varepsilon_{n+1}^{el}\} = \{\varepsilon_n^{el}\} + \{\Delta\varepsilon^{el}\} \\ \{\Delta\varepsilon^{pl}\} + \{\varepsilon_{n+1}^{el}\} = \{\Delta\varepsilon\} + \{\varepsilon_n^{el}\} \end{cases} \quad (10)$$

Defining the variable  $\{\varepsilon^*\}$  as the sum of the elastic strain at the beginning of the increment and the fixed increment of total strain, so that:

$$\{\varepsilon^*\} = \{\Delta\varepsilon\} + \{\varepsilon_n^{el}\} \quad (11)$$

In the figure 2, the plastic modulus  $E_p$  is shown to be defined by the ratio:

$$E_p = \frac{\overline{\sigma}}{\Delta\varepsilon^{pl}} \quad (12)$$

Equation (7) can now be written as a function of the plastic modulus in which  $\dot{\varepsilon}^{pl}$  is replaced by  $\Delta\varepsilon^{pl}$ :

$$\{\Delta\varepsilon^{pl}\} = \frac{1}{E_p} [P] \{\sigma\} \quad (13)$$

The relation between the elastic strain and stress is expressed by:

$$\{\varepsilon^{el}\} = [C^{el}]^{-1} \{\sigma\} \quad (14)$$

Using equation (13) and (14), the stress can be calculated as a function of  $\{\varepsilon^*\}$ :

$$\{\sigma\} = \left( \frac{1}{E_p} [P] + [C^{el}]^{-1} \right)^{-1} \{\varepsilon^*\} \quad (15)$$

Let us defined the elasto-plastic tensor  $[C^{ep}]$  as:

$$[C^{ep}] = \left( \frac{1}{E_p} [P] + [C^{el}]^{-1} \right)^{-1} \quad (16)$$

For the graphical representation of Figure 3, equation 15 is now rewritten as:

$$\left( \frac{1}{E_p} [C^{el}] [P] \right) \{\sigma_n\} + \left( \frac{1}{E_p} [C^{el}] [P] + [1] \right) \{\Delta\sigma\} = [C^{el}] \{\Delta\varepsilon\} \quad (17)$$

Figure 3 shows a representation of this relationship where the right term is the elastic prediction.

For one increment, the stress path (and strain path) are proportional to  $E_p$ .

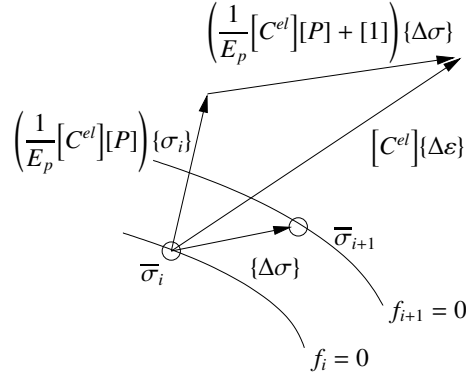


Figure 3: Stress path for incremental deformation theory

The increment of equivalent plastic strain must now be determined to compute  $\{\sigma\}$ . This is done in the following manner.

As the increment of equivalent plastic strain energy is equal to the increment of plastic strain energy:

$$\sigma_{eq} \Delta \bar{\varepsilon}^{pl} = \langle \sigma \rangle \{ \Delta \varepsilon^{pl} \} \quad (18)$$

A straightforward combination of equations (7) and (18) shows that the equivalent plastic increment is:

$$\Delta \bar{\epsilon}^{pl} = \left( \langle \Delta \epsilon^{pl} \rangle [P^{-1}] \{ \Delta \epsilon^{pl} \} \right)^{1/2} \quad (19)$$

Similarly the elastic strain energy is defined by:

$$\Delta \sigma_{eq} \Delta \bar{\epsilon}^{el} = \langle \Delta \sigma \rangle \{ \Delta \epsilon^{el} \} \quad (20)$$

In this work, it is assumed that the elastic anisotropy characteristic is approximately equal to the plastic one. This hypothesis is frequently used for calculations in the Inverse Approach (one step method) as done, for example, by Naceur et al. (2004). Therefore :

$$[C^{el}] = E [P^{-1}] \quad (21)$$

Referring to uniaxial loading, the stress and elastic strain increments are linked by the following relation:

$$\Delta \sigma_{eq} = E \Delta \bar{\epsilon}^{el} \quad (22)$$

Combining equations (1) and (21) with (22), the equivalent elastic strain increment is found to be:

$$\Delta \bar{\epsilon}^{el} = \left( \langle \Delta \epsilon^{el} \rangle [P^{-1}] \{ \Delta \epsilon^{el} \} \right)^{1/2} \quad (23)$$

As per the three-dimensional case, the partition of the equivalent strain  $\Delta \bar{\epsilon}$  into plastic and elastic parts leads to the following additive relationship:

$$\Delta \bar{\epsilon} = \Delta \bar{\epsilon}^{el} + \Delta \bar{\epsilon}^{pl} \quad (24)$$

Combining equations (19) and (23) with (24), the equivalent total strain increment is found to be:

$$\Delta \bar{\epsilon} = \left( \langle \Delta \epsilon \rangle [P^{-1}] \{ \Delta \epsilon \} \right)^{1/2} \quad (25)$$

Given the aforementioned assumptions, it is now possible to obtain the increment of equivalent plastic strain by solving equation (5) using the Newton-Raphson algorithm:

$$\bar{\sigma}_{k+1} = A + B \left( C + \bar{\varepsilon}_k^{el} + \Delta \bar{\varepsilon} - \frac{\bar{\sigma}_{k+1} - \bar{\sigma}_k}{E} \right)^n \quad (26)$$

In (26), the subscript  $k$  represents the state at the beginning of the increment, and  $k + 1$  the state at the end of the increment.

#### 4. Sheet metal forming applications

In order to compare the two plastic material deformation algorithms, previously discussed, in the same computing conditions, both the classical flow rule and new incremental deformation approach were implemented in the commercial FE code ABAQUS Explicit. The two algorithms were developed in user material subroutines (VUMAT). In the Flow Rule Formulation (FRF) (figure 4), the strain and stress tensors are computed at each iteration in the plastic loop. In the Incremental Deformation Formulation (IDF) (figure 5), only the equivalent stress is computed at each iteration.

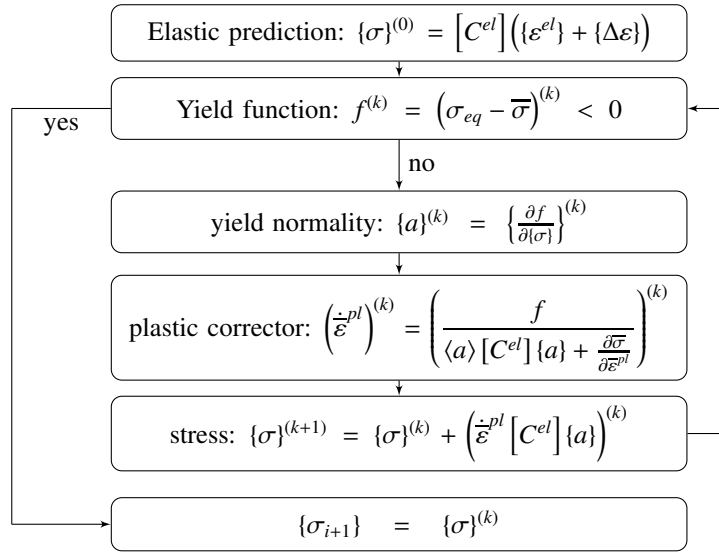


Figure 4: Flow rule algorithm

In the following, the two algorithms are tested and compared using :

- Only one point representing an elementary homogeneous volume with a significant change in the strain path,

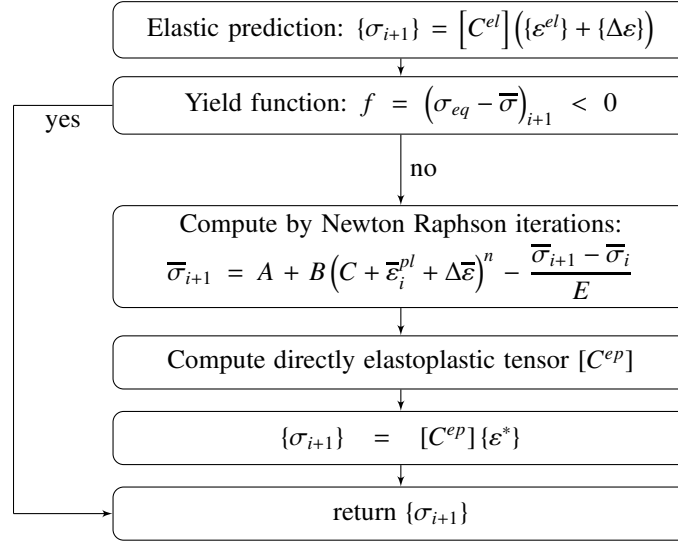


Figure 5: Incremental deformation algorithm

- the Nakazima Test for the simulation of a typical stretch forming operation,
- the incremental single point forming process of a cylindrical cup.

#### 4.1. Elementary homogeneous volume

A comparison is initially done without using a finite element analysis. The material behavior laws are integrated in a specifically written FORTRAN program which uses the imposed strain path as an entry. The calculation is done for a point subject to a state of plane stress.

Consider a point that exhibits elasto-plastic material behavior, with the following parameters :

- Young's Modulus = 96000 MPa
- Poisson's ratio = 0.33

Isotropic hardening using the Swift law :

$$\sigma_y = 150 \left( 0.013 + \bar{\varepsilon}^{pl} \right)^{0.214} MPa \quad (27)$$

The imposed strain is initially uniaxial, where the strain tensor is given by:

$$\varepsilon_1 = \langle 0.5; 0; 0 \rangle \quad (28)$$

The point is then subject to shear, while keeping the uniaxial strain already imposed.

$$\varepsilon_3 = \langle 0; 0; 0.5 \rangle \quad (29)$$

Figure 6 shows the stress path in the principal coordinate system. The flow rule theory is used. Several zones can be observed :

- Between points A and D: the strain  $\varepsilon_1$  is applied.
- Between points D and F: the strain  $\varepsilon_2$  is added to  $\varepsilon_1$ .
- Between points A and B: the behaviour is purely elastic, the stress follows a line in the direction  $(\nu; 1)$ .
- Between the points B and C: the behavior goes from being purely elastic to being quasi purely plastic. If the Young's modulus was lower, point C would be subject to a higher principal stress  $\sigma_I$  than the values determined in the present case
- Between the points C and D: The plastic strain is much higher than the elastic strain. The behavior is close to that of purely elastic behavior. The stress state follows a line in the direction  $(0.5; 1)$ .
- Between the points D and E: the behavior goes from being uniaxial strain to a pure shear state. An evolution of the hardening occurs.
- Between points E and F: The shear stress is predominant, it follows a line in the direction  $(-1; 1)$ .

Figure 7 shows the difference between the two theories. Good correspondence can be seen between the two curves. However, a slight instability occurs when using the incremental deformation theory near point D.

To evaluate the difference in CPU time necessary to resolve this problem, the calculations have been done 1000 times in a loop, in order to achieve reasonable calculation times. The relative reduction in CPU time can be written as :

$$\delta = \frac{t^{fr} - t^{id}}{t^{fr}} \quad (30)$$

where  $t^{fr}$  denote the CPU time using the flow rule method and  $t^{id}$  the CPU time using the incremental deformation theory.

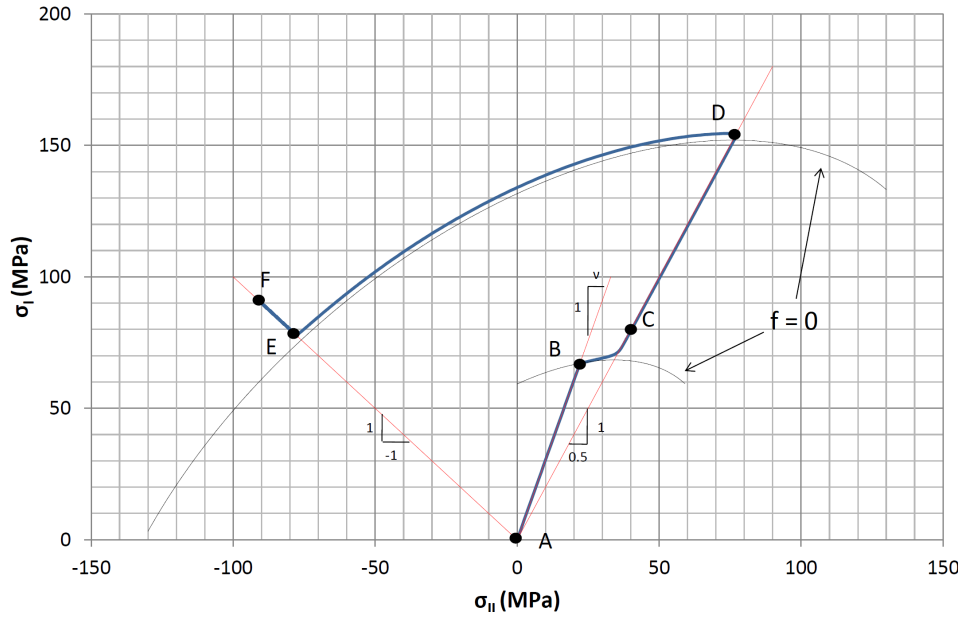


Figure 6: Stress path

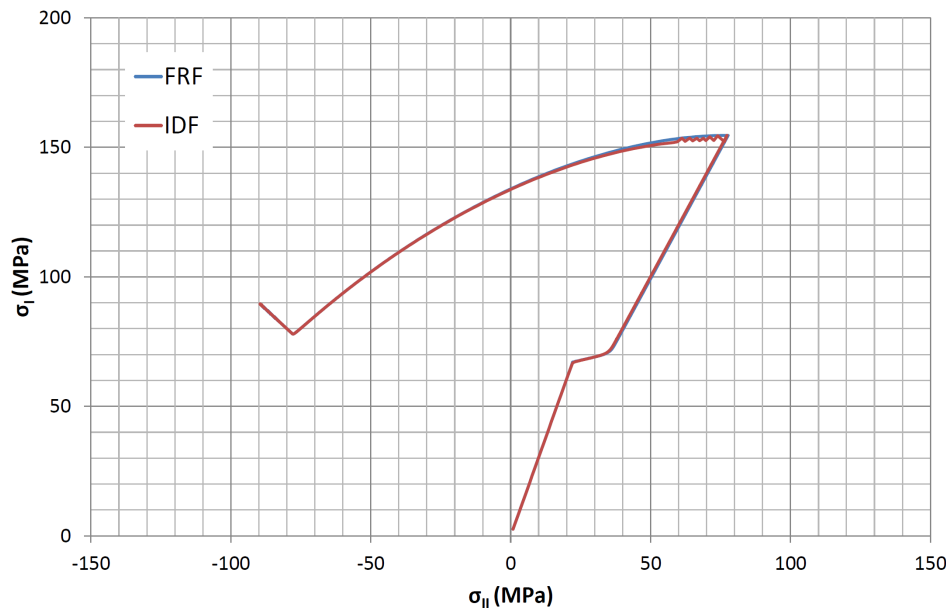


Figure 7: Comparison of the stress evolution for the two theories

In this case a reduction of 77.2% is achieved. The incremental deformation theory results in good prediction of the multiaxial stress state with a non-proportional strain path. The incremental deformation theory works well when the strain path changes significantly.

#### 4.2. Nakazima test

The Nakazima test Nakazima et al. (1968) is currently used for the experimental identification of Forming Limit Curves (FLC) in stretch forming. Knockaert (2001) has experimentally studied FLC with this test. He reports that there is good agreement between the experimental results and FE simulations using the classical flow rule method in terms of the final state of principal strain. Ben Ayed (2005) has numerically studied necking criterion using the Nakazima test with the material used by Knockaert. He reports a good agreement for the necking prediction between the experimental results and FE simulations using the classical flow rule. In this work, the Nakazima test has been chosen as it is a typical stretch forming operation. Numerical comparisons, in terms of final stress state, sheet thickness and CPU time, between the two different algorithms are presented.

The material parameters identified by Ben Ayed (2005) concerning an aluminium alloy are used as material data in the numerical simulations. Their values are listed in table 1.

E (GPa)	$\nu$	$r_0$	$r_{45}$	$r_{90}$	A (MPa)	B (MPa)	C	n
70	0.3	0.45	0.85	0.35	26	466	0.0031	0.293

Table 1: Materials properties for Nakazima test

During simulation of the forming process, the clamping force applied to the sheet-metal by the blank-holder and the die is 100 kN. The punch diameter is 75 mm and the geometrical parameters of the initial flange and the die are shown in Figure 8. The friction conditions at the contact between the deformed sheet, the blankholder and the die are modelled by Coulomb law with a friction factor of 0.06. In the other contact zones the friction is neglected. The dynamic explicit solver is used.

The results of numerical simulations, using the two abovementioned formulations, are compared for a punch displacement of 40 mm. This punch displacement experimentally leads to necking of the part. Triangular, three nodes, shell finite elements are used (S3R) with 5 Simpson integration points in the thickness direction. The global element size is approximately 3 mm and the model has 13086 degrees of freedom. The tooling is modelled by analytic rigid surfaces. Figure 9 shows the

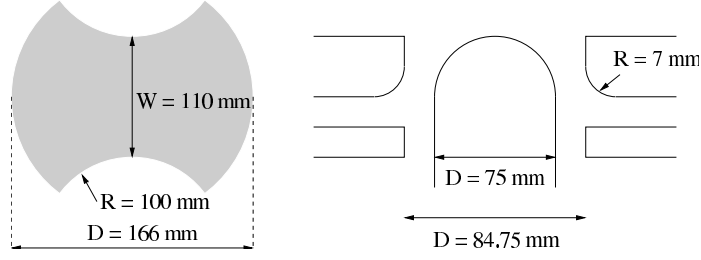


Figure 8: Flange and geometrical parameters for Nakazima test

final shape with the equivalent plastic deformation in the middle surface at the end of the forming operation using the classically flow rule method.

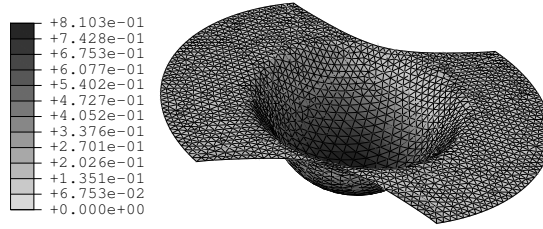


Figure 9: Final shape with equivalent plastic deformation at the end of forming with flow rule method

Table 2 shows the relative difference between maximum stresses and plastic deformation, minimum sheet thickness and CPU time obtained by both theories. The classical flow rule approach is used as the reference case. The relative difference is defined by the general formula:

$$\delta\% = 100 \left| \frac{()^{fr} - ()^{id}}{()^{fr}} \right| \quad (31)$$

where the superscripts *fr* denote the flow rule method and *id* the incremental deformation theory.

It can be noted that the incremental deformation theory produces a significant reduction in CPU time and good agreement with the flow rule theory for the simulation results. The time benefit for the complete simulation and the number of plastically deformed elements are plotted as a function of the punch displacement in Figure 10.

The total time benefit increases as the number of plastically deformed elements increases. At the end of the forming operation there is a small drop in the time benefit, even though the number of plastic elements remains basically constant.

	Flow rule	Incremental deformation	Relative difference (%)
CPU time	3h19min	2h52min	13.3
Stress max	465.0 MPa	464.2 MPa	0.17
Plastic strain max	0.813	0.801	1.48
Thickness min	0.373 mm	0.375 mm	0.536

Table 2: Nakazima test results for the aluminium alloy

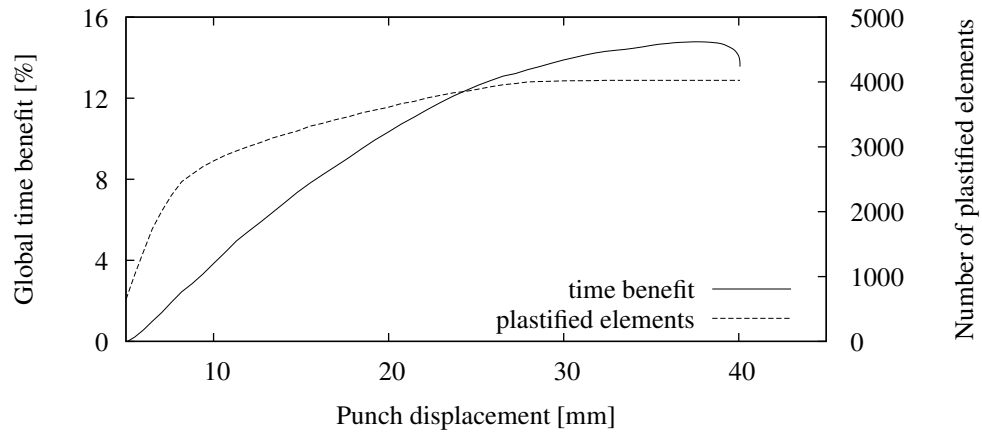


Figure 10: Time benefit and number of element in plastic domain for Nakazima test

In order to have more details about the time benefit, the evolution of the CPU time and the number of elements in plastic domain between two small punch displacements are studied. The tool displacement is a function of the loading time in the FE model. If  $t_f$  is the final loading time, the time increment for a tool displacement ( $t_i^{td}$ ) is defined by equation (28). This time increment is a result of the post-processing and not the time increment of the dynamic explicit solver (which is much smaller).

$$t_i^{td} = t_{i-1}^{td} + \frac{t_f}{100} \quad (32)$$

Let  $t_i^{fl}$  and  $t_i^{id}$  the CPU time to go to the time  $t_i^{td}$ . The superscript *fl* refers to the flow rule method and *id* for the incremental deformation theory. The incremental time benefit (ITB) is defined as (see Figure 11):

$$ITB_i(\%) = 100 \left( \frac{(t_i^{fl} - t_{i-1}^{fl}) - (t_i^{id} - t_{i-1}^{id})}{t_i^{fl} - t_{i-1}^{fl}} \right) = 100 \left( \frac{\Delta t^{fr} - \Delta t^{id}}{\Delta t^{fr}} \right) \quad (33)$$

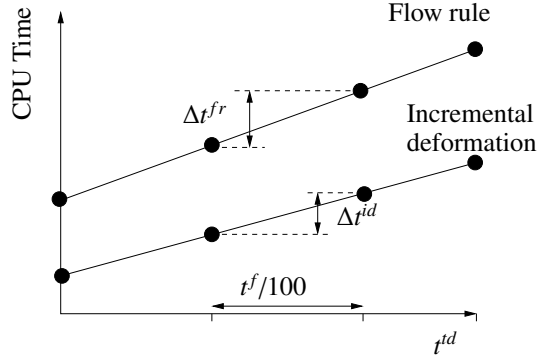


Figure 11: CPU time for one time increment for a tool displacement

The incremental plastified elements (IPE) at time  $t_i$  is defined as the number of elements who have increased the equivalent plastic strain between  $t_{i-1}$  and  $t_i$ .

Figure 12 shows the change in time benefit and the change in the number of plastic elements (IPE) plotted as functions of the punch displacement.

As per Figure 10, Figure 12 shows that the time benefit is significant if there are a large number of elements in plastic domain. Three zones can be identified in this figure. In the first zone (at the

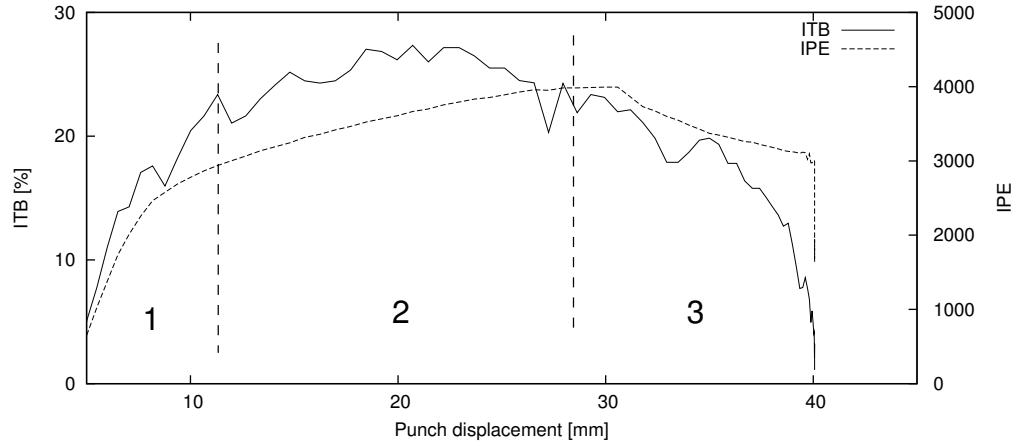


Figure 12: ITB and IPE for Nakazima test

beginning of the operation), there is an increasing degree of contact and material behaviour non-linearity, consequently the time benefit increases. In the second zone, the material behaviour is the major source of non-linearity, and the time benefit is approximately 25%. In the final zone, the non-linearity due to large strain and contact is the principal source of non-linearity, hence the time benefit decreases.

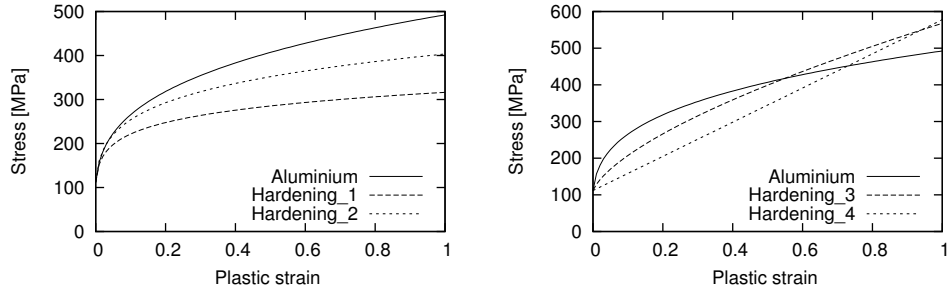


Figure 13: Different hardening law for Nakazima test

The hardening law used in this study has been defined in equation 5  $(\bar{\sigma} = A + B(C + \bar{\epsilon}^{pl})^n)$ . Different value of the hardening exponent  $n$  have been investigated in order to determine the sensitivity of the time benefit, and the quality of results. The materials parameters have been computed in order to keep a constant initial yield stress, thus the parameter  $A$  value may be negative. The parameters

values are shown in Table 3 and the resulting stress-strain curves are plotted in Figure 13. The elastic material parameters, the Lankford parameters, and the process parameters are the same as in the previous case.

	$A$ (MPa)	$B$ (MPa)	$C$	$n$
Aluminium	26.0	466.0	0.0031	0.293
Hardening_1	-149.8	466.0	0.0031	0.1
Hardening_2	-62.78	466.0	0.0031	0.17
Hardening_3	100.9	466.0	0.0031	0.65
Hardening_4	110.3	466.0	0.0031	1.0

Table 3: Hardening parameters for Nakazima test

The results of this sensitivity analysis are show in Table 4. For each simulation, the relative differences (with the classical flow rule method used as the reference) are in the same order of magnitude.

	Relative difference (eq. 31) of			
	Equivalent stress max (%)	Equivalent plastic strain max (%)	Thickness min (%)	CPU time (%)
Hardening_1	0.012	0.091	0.076	12.6
Hardening_2	0.021	0.107	0.123	13.0
Hardening_3	0.077	0.174	0.101	13.6
Hardening_4	0.043	0.156	0.075	14.3

Table 4: Nakazima test results for different hardening parameter  $n$

As seen in the Table 4 and Figure 14, the time benefit increases slightly when the hardening exponent  $n$  increase. The maximum benefit occurring when  $n = 1$  (Hardening\_4). However, the degree of non-linearity of the hardening law does not have a large influence of the total simulation time. The evolution of this time is the same for the both theories.

#### 4.3. Cup test in Incremental Sheet Forming

In this section, the Single Point Incremental Forming (SPIF) of a cylindrical cup will be analysed. This forming process is generally carried out on CNC machine-tools like grinding or milling

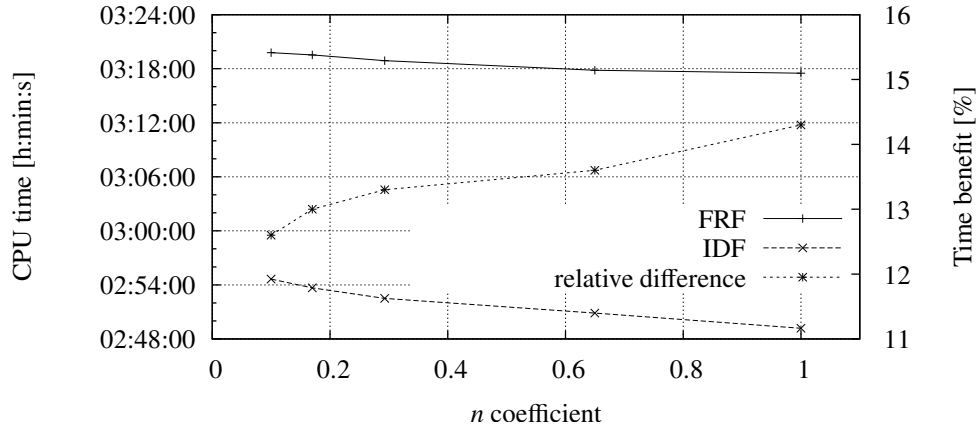


Figure 14: CPU time, and time benefit with Nakazima test

machines. The punch is a smooth ended rod with a hemispherical head and it is moved along a path, enforcing the sheet-metal.

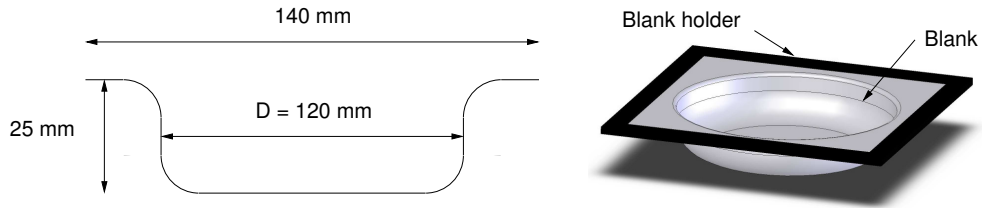


Figure 15: Geometry and blank holder of the cup

The benchmark, on which the comparison of the performances of the plastic flow rule and incremental deformation formulation is based, was proposed by Bambach et al. (2007). A square flange of aluminium alloy is clamped on its periphery by means of a blankholder and it is formed to the desired shape by the punch acting on the upper surface of the sheet-metal. The geometry of the cup is showed on figure 15.

The sheet and tools dimensions as well as the material properties are presented in table 5. The tool path is a five circle pocket as showed on figure 16.

The flange is modelled in Abaqus by finite elements of shells with 4 nodes, reduced integration (S4R) and 9 Simpson integration points in the thickness direction. The global size of elements is  $2 \times 2$  mm and the model has 30525 degrees of freedom. The tool which is much stiffer than the sheet

Geometrical dimensions (mm)	Initial sheet length	Cup depth	Cylindrical cup diameter	Sheet thickness	Hemispherical punch diameter
	140	25	120	1.5	30
Material properties	$E$ (GPa)	$\nu$	$K$ (MPa)	$n$	$\varepsilon_0$
	69	0.3	150	0.214	0.013

Table 5: Geometrical dimensions and material properties for cup test (incremental sheet forming)

is modelled by an analytic rigid surface. The blankholder is modelled by boundary conditions on the flange in which all degrees of freedom (displacements and rotations) are fixed.

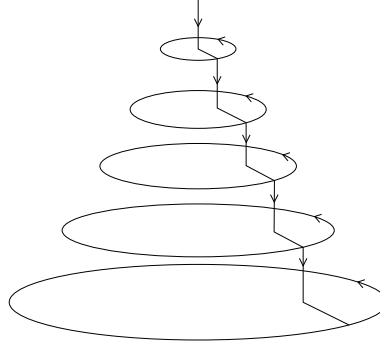


Figure 16: Tool path of the cup

The equivalent plastic deformation and the tool position during the simulation of forming (25 mm depth) is presented in Figure 17 using the classical flow rule method.

The results of the forming operation simulation are reported in Table 6, at the end of the forming.

Comparing the results obtained by means of the two formulations, the advantage of IDF on FRF is not significant. A small reduction of the CPU time simulation is observed probably due to the low number of elements concerned by the plastic deformation zone at a given time. This is a characteristic point of the SPIF process for which the diameter of the tool is small compared to the sheet dimensions. The reduction of the computation time when using the IDF is plotted in Figure 18 as a function of the tool displacement.

The effective CPU time benefit seems to be not significant in case of SPIF. Its maximum value is reached during the last circular tool path which begins at approximately 65% of the total displace-

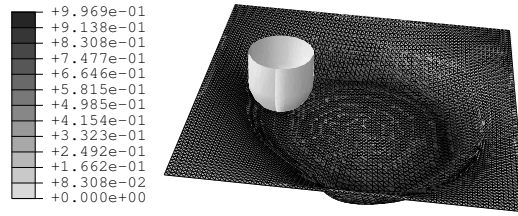


Figure 17: Equivalent plastic strain forming with flow rule method and the tool during forming

	Flow rule	Incremental deformation	Relative difference (%)
CPU time	6h48min	6h30min	4.3
Stress max (MPa)	144.9	143.6	0.91
Plastic strain max	0.9976	0.9988	0.12
Thickness min (mm)	0.573	0.572	0.17

Table 6: Cup test results for incremental sheet forming of aluminium alloy

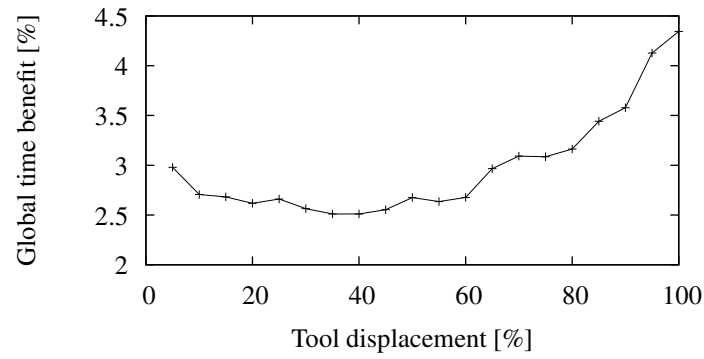


Figure 18: Time benefit with cup test

ment. The time benefit increases during this last forming operation because most of the elements lie in the plastic domain where the IDF exhibit its major advantage on the FRF.

The results between both theories are compared for two sections on the geometry, before and after the pulling up of the punch. These paths are shown on figure 19.

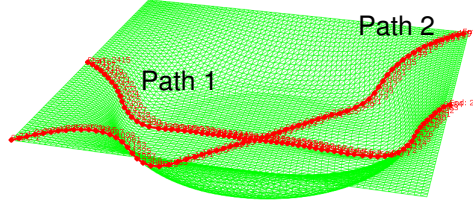


Figure 19: Post-treatment path for the cup test

Figure 20a show the z displacement for path 1 and figure 20b for path 2. The non-constant depth on figure 20a is due the z-tool displacement after each circle tool path. For path 2, the depth is approximately constant. A good geometry is observed for the IDF, compared with the FRF. For both paths, the observed springback value is approximately 1 mm.

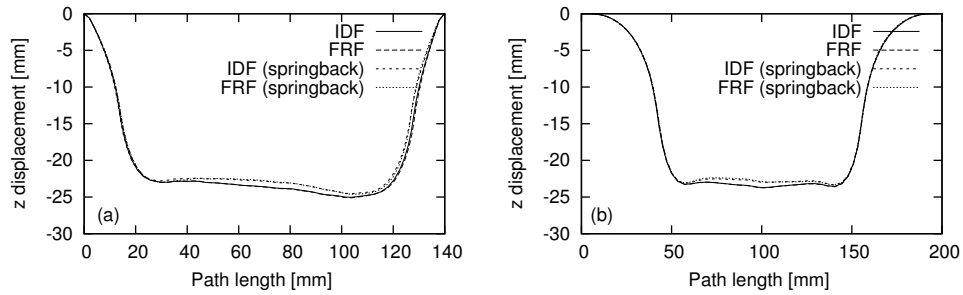


Figure 20: z-displacement for path 1 (a) and path 2 (b)

Figure 21a shows the thickness for path 1 and figure 21b for path 2. A good thickness prediction is observed for the IDF, compared with the FRF.

During that process, it is possible that a material point undergo several elasto-plastic states followed by elastic unloading. The results comparison shows that the IDF is able to take into account complex elasto-plastic loading and unloading.

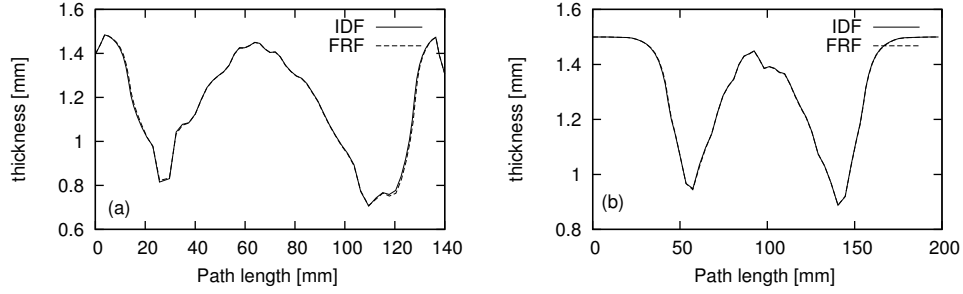


Figure 21: Final thickness for path 1 (a) and path 2 (b)

## 5. Conclusion

The incremental deformation theory and the flow rule plasticity method are investigated in case of forming anisotropic sheet-metal. The elasto-plastic formulations for both theories which include the Hill 48 criterion are implemented into the commercial FE code ABAQUS EXPLICIT. The algorithms were developed and introduced via user material subroutines (VUMAT). The numerical performances of both theories are compared in the same computing conditions in the case of two sheet-metal forming benchmarks.

These two algorithms are first tested on a material point with a significantly change in the strain path. The behavior is the only one non-linearity. A large reduction of the CPU time (more than 70%) for the incremental formulation theory is observed, compared to the flow rule formulation, with a good prediction of the multiaxial stress state.

A stretch forming of a spherical cup was first modelled as a forming example in which the contact conditions between the tools and the sheet are dominant. It was found that the incremental deformation formulation gave good results compared to the flow rule formulation. A significant reduction of the CPU time is observed with IDF. The time benefit reaches its maximum at half time of the forming operation because the material non-linearity is dominant.

In the second situation, the single point incremental forming of a cylindrical cup was tested. In that case, the localized contact zone between the tools and the sheet is following the tool path all along the forming operation. It was found that the time benefit was small (only 4%), however good results are observed. The incremental deformation theory has not an important impact with this process. This is explained by the localization of the contact between the tool and the sheet (high contact non-

linearity), and the small tool diameter compared with the sheet dimensions (few elements are in the plastic domain at a given time).

It can be concluded that the major advantage of the new approach is the time benefit when the material non-linearities are dominant. Contact non-linearities can significantly reduce the global time benefit obtained with this formulation. Also, this formulation works well when the strain path changes significantly under multiaxial stress state.

## References

- M. Bambach, M. Cannamela, M. Azaouzi, G. Hirt and J.-L. Batoz, 2007. Computer-aided tool path optimization for single point incremental sheet forming. *Advanced Methods in Material Forming*, 233-250, Springer Verlag., (ISBN 978-3-540-69844-9).
- L. Ben Ayed, 2005. Modélisation numérique de l'emboutissage et l'optimisation des outils serre-flanc. Ph.D. thesis, Université de Technologie de Compiègne, France.
- K. Chung and O. Richmond, 1993. A deformation theory of plasticity based on minimum work paths. *International Journal of Plasticity* 9 (8), 907-920.
- M.A. Crisfield, 1991. *Non-Linear Finite Element Analysis of Solids and Structures*. Vol. 1. John Wiley & Sons Ltd.
- Y. Q. Guo, J. L. Batoz, H. Naceur, S. Bouabdallah, F. Mercier and O. Barlet, 2000. Recent developments on the analysis and optimum design of sheet metal forming parts using a simplified inverse approach. *Computers & Structures* 78 (1-3), 133-148.
- Y. Q. Guo, Y. M. Li, F. Bogard and K. Debray, 2004. An efficient pseudo-inverse approach for damage modeling in the sheet forming process. *Journal of Materials Processing Technology* 151 (1-3), 88-97.
- Hencky, H., 1924. Zur Theorie plastischer Deformationen und der hierdurch im Material hervorgerufenen Nachspannungen. *ZAMM - Journal of Applied Mathematics and Mechanics* 4 (4), 323-334.
- R. Knockaert, 2001. Numerical and experimental study of the strain localization during sheet forming operations. Ph.D. thesis, Ecole Nationale Supérieure des Mines de Paris, France.

- J. Lemaitre and J.-L. Chaboche, 1988. *Mécanique des matériaux solide*. Bordas.
- V.A. Lubarda, 2000. Deformation theory of plasticity revisited. *Proc. Mont. Acad. Sci. Arts* 13, 117-143.
- J. Na, J. Jiao, Y. Yan and H. Liu, 2011, A membrane element model with bending modification for one step inverse method. *Acta Mechanica Solida Sinica* 24 (3), 282-288.
- H. Naceur, A. Delaméziere, J. L. Batoz, Y. Q. Guo and C. Knopf-Lenoir, 2004. improvements on the optimum process design in deep drawing using the inverse approach. *Journal of Materials Processing Technology* 146 (2), 250-262.
- K. Nakazima, T. Kikuma and K. Hasuka, 1968. Study on the formability of steel sheets. Yamata Technical Report 264, 141 - 154.
- N. Ramakrishnan, Krishna M. Singh, R.K.V. Suresh and N. Srinivasan, 1998. An algorithm based on total-elastic-incremental-plastic strain for large deformation plasticity. *Journal of Materials Processing Technology* 86 (1-3), 190-199.
- J.C. Simo and M. Ortiz, 1985. A unified approach to finite deformation elastoplastic analysis based on the use of hyperelastic constitutive equations. *Computer Methods in Applied Mechanics and Engineering* 49 (2), 221-245.
- D.Y. Yang and Y.J. Kim, 1986. A rigid-plastic finite-element formulation for the analysis of general deformation of planar anisotropic sheet metals and its applications. *International Journal of Mechanical Sciences* 28 (12), 825-840.